Proceedings Ninth Workshop Geothermal Reservoir Engineering
Stanford University, Stanford, California, December 1983
SGP-TR-74

PERMEABILITY REDUCTION DUE TO PRECIPITATION OF QUARTZ UNDER NONISOTHERMAL CONDITIONS

Laura A. Keith[1], Paul T. Delaney[1], and Diane E. Moore[2]

[1] U.S. Geological Survey
2255 North Gemini Dr.
Flagstaff, Ariz., 86001

[2] U.S. Geological Survey
345 Middlefield Rd.
Menlo Park, Calif., 94025

ABSTRACT. Many problems concerning the origin and exploitation of geothermal reservoirs demonstrate the need for models of reactive-solute transport. Of particular interest to us is the coupling between dissolution/precipitation reactions and transient-flow behavior. In an effort to account for observed flow-rate reductions during experiments on samples of granite held in a temperature gradient (summarized at this meeting in 1981 by Moore and others), we examine the effect of quartz precipitation on fluid flow. Our results confirm earlier inferences that reactions responsible for porosity reduction were affected by kinetic factors. Although our results show substantial flow-rate reductions, we are unable to reproduce measured silica concentrations of the outlet fluid by considering the behavior of silica phases without regard for that of the feldspars and micas.

INTRODUCTION. It is well established that quartz dissolves readily in geothermal and other hydrothermal settings. Silica precipitation, however, may be responsible for hydraulic seals in some reservoirs (Facca and Tonani, 1967). In a recent series of papers on simultaneous fluid, heat and mass transfer in granites (Summers and others, 1978; Lockner and others, 1978; Morrow and others, 1981; Moore and others, 1981, 1983), such processes were observed in a laboratory setting. These experiments were performed on cylindrical samples of the Westerly and Barre Granites, bounded by endpieces of fused silica (fig. 1). Distilled water was pumped into axial boreholes, which housed heater coils. Temperatures of 250° or 300°C were maintained at the inside of the sample; stable values of 84° to 103°C were recorded at the outside. Fluid-pressure differences of 0.5-1.0 MPa were maintained between the axial reservoir and the outside of the sample. Mass flux of water and various dissolved species were monitored over a period of a few weeks, and flow-rate reductions were observed (fig. 1). Concentrations of dissolved silica in the outlet fluid were typically, but not always, supersaturated with respect to amorphous silica in experiments with 250°C axial temperatures, whereas only quartz supersaturation was observed in experiments with 300°C temperatures. The pH of outlet fluids was neutral. Moore and coworkers concluded that quartz was the primary phase to precipitate, thus inducing flow-rate reductions.

Figure 1. Sketch of sample apparatus; graphs of mass fluid flux and aqueous silica concentration versus time for experiments 1, 2, 3 and 4, corresponding to B250-2, B300, W250 and W300, respectively, of Moore and others (1983). Conditions of experiments and dimensions of granite annulus are given in table 2. Flow rates are normalized by their initial values. Gibbs free energies of reaction ΔG_r, in kcal, are shown for the final fluid samples collected.

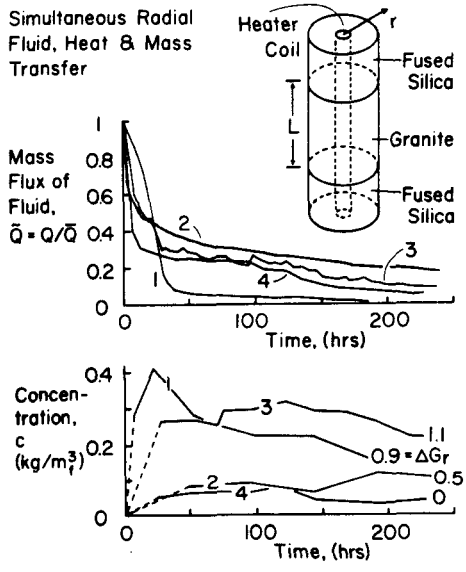

The purpose of this paper is to test the hypothesis that the reaction

$$SiO_2 + 2 \cdot H_2O \rightleftharpoons H_4SiO_4$$

where quartz and water combine to form aqueous silica is responsible for the hydraulic sealing of the samples. This hypothesis requires that the role of other silica phases, feldspars and micas in the overall mass transfer was unimportant. Li (1980) investigated a similar problem.

HEAT TRANSFER. Consider the energy equation:

$$(\rho C)\frac{\partial T}{\partial t} = \frac{1}{r}\frac{\partial}{\partial r} rk\frac{\partial T}{\partial r} + (\rho C)_f v \frac{\partial T}{\partial r} + (\Delta h)R \qquad (1)$$

which balances the accumulation of heat (LHS)

Table 1: Symbols and their Dimensionless Equivalents.

a Area of reaction surface;

c Concentration, $\zeta = c/\overline{s}_q$;

C Heat capacity, per unit mass;

G Reaction-rate group, $\overline{\phi}\overline{\mu}r_b^2\overline{a}_q\overline{k}_-/\overline{K}(P_a-P_b)\overline{m}_f$;

h Enthalpy of reaction;

k Thermal conductivity, $\tilde{k} = k/\overline{k}$, $\tilde{k}_0 = k_0/\overline{k}$, $\tilde{k}_1 = k_1/\overline{k}$;

k_- Precipitation rate constant, $\tilde{k}_- = k_-/\overline{k}_-$;

K Absolute permeability, $\tilde{K} = K/\overline{K} = \phi^3$;

m Mass of fluid available for reaction;

Q Fluid flux, $\tilde{Q} = Q/\overline{Q} = Q\cdot\overline{\mu}/2\pi L\overline{\rho}_f\overline{K}(P_a-P_b)$;

r Radial distance, $\eta = r/r_b$;

R Kinetic reaction rate;

P Pressure, $\psi = (P-P_b)/(P_a-P_b)$;

s Solubility, $\tilde{s} = s/\overline{s}_q$;

T Temperature, $\theta = (T-T_b)/(T_a-T_b)$, $\theta_1 = (273.15^oC+T_b)/(T_a-T_b)$;

t Time, $\tau = t/T$, $T = \overline{\phi}_f\overline{\mu}r_b^2\rho_q/\overline{K}(P_a-P_b)\upsilon_q\overline{s}_q$;

v Darcian velocity, $\tilde{v} = v/\overline{v} = v\cdot\overline{\mu}r_b/\overline{K}(P_a-P_b)$;

α Dispersivity, $A = \alpha/r_b$;

ϕ Volume fraction, $\Phi = \phi_f/\overline{\phi}_f$;

ρ Density, $\tilde{\rho} = \rho_f/\overline{\rho}_f$;

μ Dynamic viscosity, $\tilde{\mu} = \mu/\overline{\mu}$;

υ Atomic-weight ratio;

Superscripts and subscripts.

a Value at $r = r_a$, inside of annulus;

b Value at $r = r_b$, outside of annulus;

f Fluid;

q Quartz;

r Value in axial reservoir;

s Amorphous silica;

- denotes properties evaluated at the inside of the sample ($r=r_a$,t) for properties that do not vary with time, or initially (r,t=0) for those that do not initially vary spatially.

Table 2: Values of Properties.

$a^r_q = 8.8 \times 10^{-4}\ m^3{}_q$; $a^r_s = 3.9 \times 10^{-3}\ m^3{}_s$;
$k_0 = 0.586\ W/m\cdot s^oC$; $k_1 = 556\ W/m\cdot s$;
$L = 8.9$ cm; $r_a = 0.64$ cm; $r_b = 3.8$ cm;
$\rho_q = 2650\ kg/m^3$; $V^r_f = 4.9 \times 10^{-6}\ m^3{}_f$;
$\upsilon_f = 0.375$; $\upsilon_q = 0.675$

	1	2	3	4	= Experiment #
	(Barre)		(Westerly)		
$\overline{k}$ =	1.65	1.56	1.65	1.56	$W/m\cdot s^oC$;
$\overline{k}_-$ =	2.12	5.76	2.12	5.76	$\times 10^{-6}\ kg_f/m^2{}_q\cdot s$;
$\overline{K}$ =	2000	74	740	240	$\times 10^{-21}\ m^2$;
P_a =	10.5	21.0	10.5	20.5	MPa;
P_b =	10.0	20.0	10.0	20.0	MPa;
$\overline{s}_q$ =	0.61	0.86	0.61	0.86	$kg_{H_4SiO_4}/m^3{}_f$;
$\overline{s}_s$ =	1.66	1.90	1.65	1.90	$kg_{H_4SiO_4}/m^3{}_f$;
T_a =	250	300	250	300	^oC;
T_b =	103	94	84	92	^oC;
$\overline{\rho}$ =	806	736	806	736	kg/m^3;
$\overline{\mu}$ =	1.08	0.91	1.08	0.91	$\times 10^{-4}$ Pa·s;

against its conduction, advection and rate of production through chemical reaction (RHS). (See table 1 for notation.) Although experiments ran for durations in excess of 100 hr, transient heating lasted less than 2 hr. Using the nondimensionalization shown in Table 1, the ratio of advective to conductive heat transfer scales as $(\rho C)_f\overline{K}(P_a-P_b)/\overline{\mu k}$ which is $<<1$; the influence of the heat of reaction is even less. Defining, nondimensional temperature θ, thermal conductivity $\tilde{k}$ and distance r/r_b, we can write the conduction equation

$$0 = \frac{1}{\eta}\frac{\partial}{\partial\eta}\eta\tilde{k}\frac{\partial\theta}{\partial\eta}\ , \text{ where } \tilde{k} = \tilde{k}_0 + \tilde{k}_1/(\theta+\theta_0) \qquad (2)$$

which reflects that thermal conductivity is inversely proportional to absolute temperature and has been fitted to data summarized by Touloukian and others (1981) for the Westerly and Barre Granites. (Values of parameters are given in table 2.) Boundary conditions are

$$\theta(r_a/r_b) = 1, \quad \theta(1) = 0 \qquad (3)$$

The solution is transcendental:

$$\tilde{k}_0(1-\theta) + \tilde{k}_1\ln[(1+\theta_0)/(\theta+\theta_0)] = \qquad (4)$$
$$[1-\ln(\eta)/\ln(r_a/r_b)]\{\tilde{k}_0+\tilde{k}_1\ln[(1+\theta_0)/\theta_0]\}$$

Transport and thermodynamic properties are insensitive to variations in the pressure and concentration observed during the experiments. Therefore, profiles of nondimensional viscosity (Watson and others, 1980), thermal con-

Figure 2. Spatial distributions of (a) normalized fluid density $\tilde{\rho}$, thermal conductivity $\tilde{k}$ and viscosity $\tilde{\mu}$, and (b) solubility of quartz $\tilde{s}_q$, chalcedony $\tilde{s}_{chal}$, α-cristobalite $\tilde{s}_{crist}$ and amorphous silica $\tilde{s}_a$, and precipitation-rate constant $\tilde{k}_-$ for conditions of experiment 3.

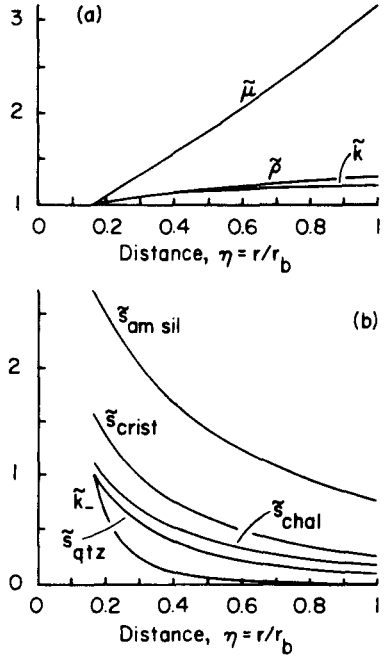

ductivity, water density (Keenan and others, 1978), silica precipitation-rate constant (Rimstidt and Barnes, 1980) and solubility of quartz, chalcedony, α-cristobalite and amorphous silica (Fournier and Potter, 1982; Fournier, personal communication, 1983) can be determined from eq. 4 alone. Figure 2 shows profiles of these quantities for the conditions of experiment 3 and for silica dissolved in otherwise pure water. Note that the spatial gradients of the solubilites and precipitation-rate constant are steepest at the heated, inside of the sample. Overall, dissolution and precipitation should be greater at the interior of the sample. Although fluids may become supersaturated with respect to α-cristobalite or chalcedony, achievement of amorphous-silica saturation is unlikely. Only the quartz-water reaction is considered here.

FLUID FLOW. The equations for conservation of momentum (Darcy's law) and fluid mass are

$$v = -(K/\mu)\frac{\partial P}{\partial r}, \quad \frac{\partial}{\partial t}\phi_f\rho_f = \frac{-1}{r}\frac{\partial}{\partial r}r\rho_f v - \upsilon_f R \quad (5)$$

Order-of-magnitude calculations for a rock with flow porosity $\phi_f = 10^{-3}$ suggest that the residence time of water in the sample was less than 1 hr, so that the term on the LHS of the second equation above is small. The addition of water by quartz precipitation (the reaction term) is also small. Thus, conservation of fluid mass is assured if the mass flux of water is constant everywhere within the sample.

We postulate that flow porosity ϕ_f of granites can be idealized as microfractures of spacing d. Permeability and porosity are related by a model of flow along these orthogonal fractures (see Turcotte and Schubert, 1982), giving

$$K \propto \phi_f^3 d^2, \quad \text{or } \tilde{K} = \Phi^3 \quad (6)$$

where $\tilde{K}$ and Φ are nondimensional permeability and porosity, respectively. Initially, the permeability function $\Phi^3 = 1$; its subsequent behavior controls flow rate and pressure. Although the porosity function is not known independently of the mass transfer and dissolution/precipitation reactions, this cube--power relation assures that minor volumes of precipitated quartz will have a significant influence on fluid flux. Other more realistic relations than eq. 6 would not alter the conclusions reached by this study.

Introducing nondimensional mass flux $\tilde{Q}$, Darcian velocity $\tilde{v}$, fluid density $\tilde{\rho}$ and pressure ψ, we find

$$\tilde{Q}(\eta,\tau) = \tilde{Q}(\tau) = \eta\tilde{\rho}\tilde{v} = -\tilde{\eta\rho}(\Phi^3/\tilde{\mu})\frac{\partial\psi}{\partial\eta} \quad (7)$$

where τ is nondimensional time. Equation 7 is solved for $\tilde{Q}$ and ψ subject to the boundary conditions

$$\psi(r_a/r_b) = 1, \ \psi(1) = 0 \quad (8)$$

THE CASE OF QUARTZ SATURATION. Conservation of silica is assured by the equation

$$\frac{1}{\upsilon_q}\frac{\partial}{\partial t}\phi_q\rho_q + \frac{\partial}{\partial t}\phi_f c = \frac{-1}{r}\frac{\partial}{\partial r}rvc + \frac{\alpha}{r}\frac{\partial}{\partial r}rv\frac{\partial c}{\partial r} \quad (9)$$

where υ_q is the atomic weight ratio of quartz to aqueous silica, α is longitudinal dispersivity and c is concentration expressed as mass of aqueous silica per volume of water. Equation 9 is derived assuming that concentration gradients across pore channels are small. Mechanical dispersion, which refers to spreading caused by microscopic variations in velocity, is the major dispersive process. If quartz is the only reactive solid, the volume fractions of quartz and water are related by

$$\partial\phi_f/\partial\phi_q = -1 \quad (10)$$

The concentration of aqueous silica may be nearly at quartz saturation throughout most of the sample. If so, then after nondimensionalizing, we have $c/\bar{s}_q = s/\bar{s}_q = \tilde{s}$ and

$$\left(1-\upsilon_q\bar{s}_q/\rho_q\right)\frac{\partial\Phi}{\partial\tau} = \frac{1}{\eta}\frac{\partial}{\partial\eta}\eta\tilde{v}\tilde{s}_q - \frac{A}{\eta}\frac{\partial}{\partial\eta}\eta\tilde{v}\frac{\partial\tilde{s}}{\partial\eta}_q \quad (11)$$

The first term in parentheses on the LHS represents the accumulation of silica as quartz; the second term, the depletion of aqueous silica due to reduced pore space, which is of the order 10^{-4} and is henceforth neglected. Nondimensional time is

$$\tau = t/T, \text{ where } T = \bar{\phi}_f \bar{\mu} r_b^2 \rho_q / \bar{K}(P_a - P_b) \upsilon_q \bar{s}_q \quad (12)$$

and is composed of an advection rate and a ratio of densities of aqueous silica and quartz. We expect that sealing occurs over times $t \sim T$ for conditions dominated by quartz-saturated fluids. Equation 11 is subject to the initial condition:

$$\Phi(\eta, \tau=0) = 1 \quad (13)$$

Because the solubility gradient is nonzero (fig. 2), any other steady state is unlikely to exist for eq. 11 than $v = 0$ and, therefore, $\Phi = 0$.

Equations 7 and 11 are solved numerically for various values of nondimensional dispersivity A (fig. 3a). Although measurements have not been made, it is inferred that $0 < A < 1$ for intact specimens. The flux of aqueous silica increases with longitudinal dispersion, and so the rate of sealing increases with A. When cast in terms of nondimensional variables, these rates do not vary substantially among the experiments. The parameter A is the only parameter acting to increase the rate of flow-rate reductions in figure 3a. For $A = 0$, nondimensional pressure is calculated across the sample at various times (fig. 3b). Pressure, as well as porosity (not plotted, but similar to figure 4e), dramatically decreases at the inside of the sample, where solubility gradients are greatest. Therefore, if pore water is saturated with quartz, the sealing is complete and occurs dominantly near the inside wall of the sample.

To compare calculated flow rates with measured ones, we have to evaluate the time-scaling factor (eq. 12), where only the initial flow porosity $\bar{\phi}_f$ is unknown. We take $\bar{\phi}_f = 10^{-3}$ and $A = 0$ to superimpose calculated curves of fluid flux versus time for experiments 1 and 3 with the measured values (fig. 3c). This comparison shows good agreement for experiment 1, but poor agreement for experiment 3. An equivalent result has been obtained by Lichtner and coworkers (1983).

KINETICALLY CONTROLLED REACTION. The kinetics of the quartz-water reaction are now included in the transport model. Because we wish to isolate kinetic effects, we only consider the case of $A \ll 1$. Conservation of aqueous silica is

$$\frac{\partial}{\partial t}\phi_f c = \frac{-1}{r}\frac{\partial}{\partial r} rvc + R \quad (14)$$

where

$$R = (\phi_f a_q / m_f) k_- (\varepsilon_q - c) \quad (15)$$

Figure 3. (a) Normalized mass fluid flux versus nondimensional time τ where $A = \alpha/r_b = 0, 0.1, 1$ for conditions of experiment 3 (solid lines); dashed line, $A = 0$ for experiments 2 and 4; dotted line, $A = 0$ for experiment 1. (b) Normalized pressure versus distance for the case of $A = 0$ and conditions of experiment 3. (c) Normalized mass fluid flux versus time for $A = 0$, $\bar{\phi}_f = 10^{-3}$ and conditions of experiments 1 and 3 as calculated from eqs. 15 and 16, and as observed.

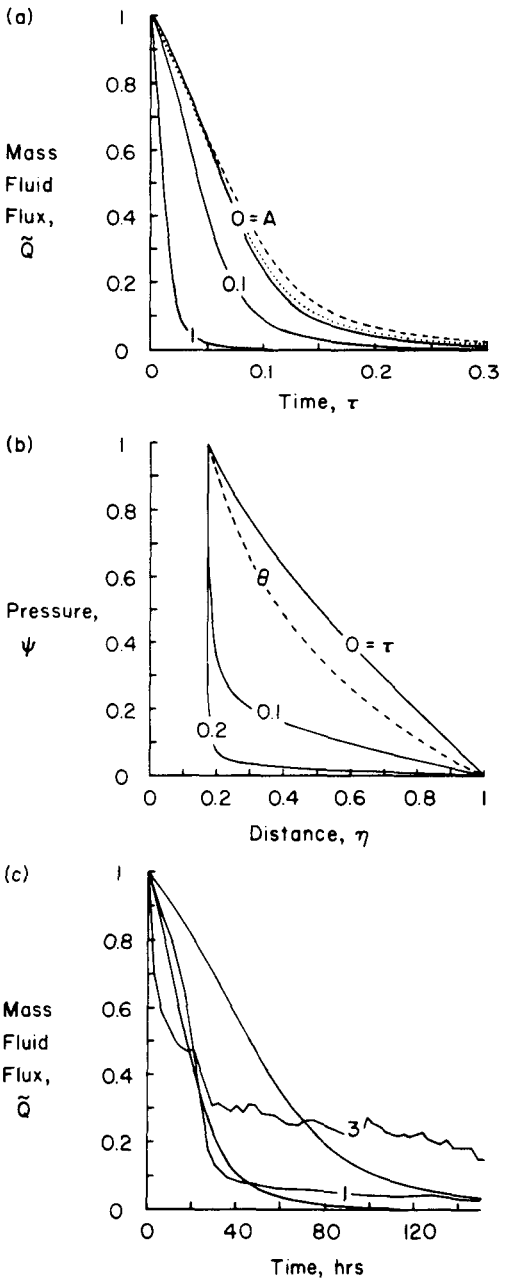

Equation 15 describes both dissolution and precipitation due to the reversible reaction between quartz and water, and aqueous silica (Rimstidt and Barnes, 1980). Although we are unaware of a rigorous development for the mass-conservation equations for nonisothermal-reacting porous media, eq. 14 is of the form discussed by Nguyen and others (1982) and Rubin (1983).

The value of the reaction parameter $\phi_f a_q / m_f$, which characterizes the extent of the reacting system, is unknown. Just as permeability can be related to flow porosity by a model of flow along orthogonal fractures, we find that

$$\phi_f a_q / m_f \propto 1/\rho_f d \qquad (16)$$

By introducing the nondimensional concentration $\zeta = c/\bar{s}_q$, eqs. 14-16 become

$$\frac{\upsilon_q \bar{s}_q}{\rho_q} \frac{\partial \phi \zeta}{\partial \tau} = \frac{-1}{\eta} \frac{\partial \eta \tilde{v} \zeta}{\partial \eta} + \frac{Gk_-}{\tilde{\rho}} (\tilde{s}_q - \zeta) \qquad (17)$$

where

$$G = \bar{\phi}_f \bar{\mu} r_b^2 \bar{a}_q \bar{k}_- / \bar{K} (P_a - P_b) \bar{m}_f \qquad (18)$$

is a ratio of kinetic-reaction rates to advection rates. For increasing values of G, the kinetics of the reaction are faster, concentrations approach saturation and the overall reaction rate becomes controlled by the advection rate. In the limit $G \to \infty$, eq. 11 is the special case $\zeta = \tilde{s}_q$ of eq. 17. Note that G is dependent upon the unknown quantities: initial flow porosity, area of quartz surface and mass of pore fluid. The LHS of eq. 17 is of the order 10^{-4} and is henceforth neglected. The boundary condition

$$\zeta(r_a/r_b) = 1 \qquad (19)$$

reflects that the inlet fluid is saturated with respect to quartz. An alternative boundary condition on concentration is incorporated below. Equation 11 (conservation of SiO_2) is

$$\frac{\partial \Phi}{\partial \tau} = \frac{1}{\eta} \frac{\partial}{\partial \eta} \eta \tilde{v} \zeta \qquad (20)$$

subject to the initial condition eq. 14.

Equations 7, 17 and 20 are solved numerically for the conditions of experiment 3 (table 2). Flow rate versus time curves (fig 4a) have

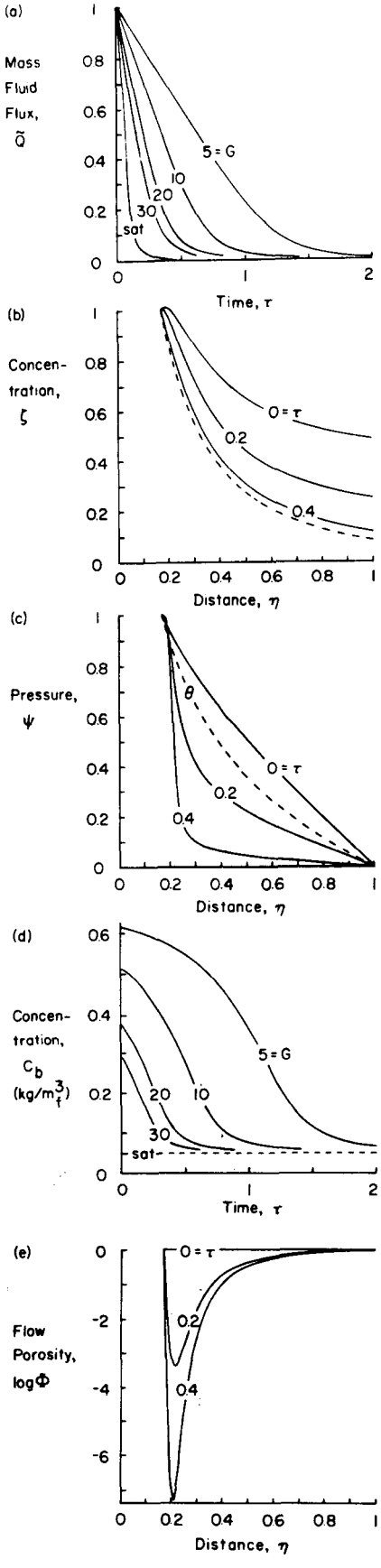

Figure 4. Inlet fluid is saturated. (a) Normalized mass fluid flux versus nondimensional time τ for G = 5, 10, 20, 30 and ∞ (saturation case, fig. 3). (b) Concentration ζ versus distance η for the case G = 30 at τ = 0, 0.2, 0.4; dashed line represents quartz solubility. (c) Pressure ψ versus η for G = 30. (d) Outlet concentration c_b versus τ for values of G. (e) Porosity Φ versus η for G = 30.

been calculated for various values of G. As G increases, the time for complete hydraulic sealing decreases. Figures 4b, 4c and 4e show how concentration, pressure and porosity, respectively, evolve in the sample over time for the case of G = 30. Concentrations approach quartz saturation only when pores are effectively sealed: that is, when pressure drops to an almost constant value throughout the sample. Porosity profiles reveal that quartz precipitates at the inside part of the sample, impeding flow from the heated reservoir. Because the inlet fluid is saturated, no dissolution of quartz occurs, and porosity only decreases from its initial value. Kinetic rates are most extreme near the high temperature end of the sample (fig. 2b) where porosity reductions are greatest. Outlet concentrations decrease steadily over time (fig. 4d) to quartz saturation, as compared to the relatively unchanging values measured (fig. 1b).

VARIABLE INLET CONCENTRATION. Although pure water was pumped into the axial reservoir, aqueous silica derived from quartz and fused silica on the reservoir wall accumulated during the course of the experiments. The presence of fused silica endpieces raises the possibility that the reservoir fluid became saturated with respect to quartz (the case above); results presented below indicate that this only occurred after complete sealing. To estimate the concentration of aqueous silica in the reservoir as a function of time, we employ the equation

$$\frac{d}{dt}c_a = \frac{-Qc_a}{\bar{\rho}_f V_f^r} + \frac{a_q^r \bar{k}}{m_f^r}(\bar{s}_q - c_a) + \frac{a_s^r \bar{k}}{m_f^r}(\bar{s}_s - c_a) \qquad (21)$$

which is a macroscopic mass balance (Bird and others, 1960, eq. 22.1-1) obtained by assuming that concentration gradients in the reservoir are small due to the presence of the heater coil. Although eq. 21 cannot be solved without knowledge of the mass flux of water into the pores (calculated from eq. 7), it nonetheless constitutes a boundary condition on the inlet concentration of aqueous silica. In nondimensional form, eq. 21 is

$$\frac{d}{d\tau}\zeta_a = \frac{-TQ\zeta_a}{\bar{\rho}_f V_f^r} + \frac{Ta_q^r \bar{k}}{m_f^r}(1-\zeta_a) + \frac{Ta_s^r \bar{k}\,\bar{s}}{m_f^r \bar{s}_q}(\zeta_a) \qquad (22)$$

Using eq. 22 and $\bar{\phi}_f = 10^{-3}$, the nondimensional time for sealing increases by more than a factor of 3 (compare figs. 4a and 5a). In the examples above, aqueous silica is introduced

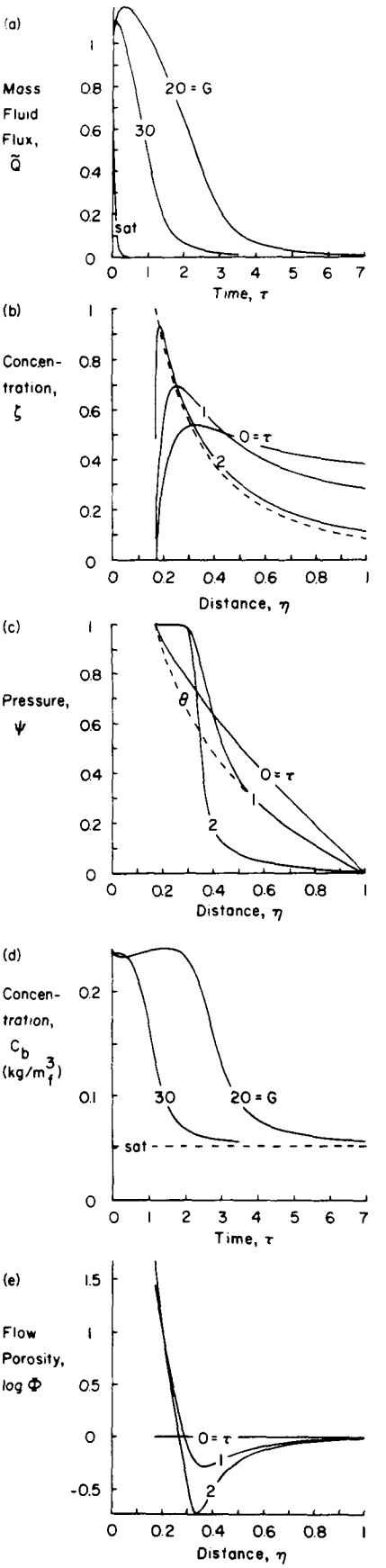

Figure 5. Concentration of inlet fluid varies with time. (a) Normalized mass fluid flux versus nondimensional τ for G = 20, 30 and ∞. (b) Concentration ζ versus distance η for the case G = 30 at τ = 0, 1 and 2. (c) Pressure ψ versus η for G = 30. (d) Outlet concentration c_b versus τ for values of G. (e) Porosity Φ versus η for G = 30.

into the samples from the reservoir; here much of the aqueous silica is derived from dissolution along pore walls, causing initial flow-rate increases. In fiqure 5b for G = 30, concentrations do not approach saturation until the sample is almost sealed ($\tau > 2$). Because dissolution occurs, pressures remain high (fig. 5c), and porosities increase at the inside of the sample (fig. 5e). As the concentration profiles intersect the quartz-solubility curve (near $\eta = 0.3$, fig. 5b), pressures and porosities correspondingly decrease due to precipitation. Outlet concentrations decrease with time (fig. 5d), although of lesser magnitude than in figure 4d, toward quartz saturation, whereas measured values do not.

CONCLUSIONS. Our results suggest that complete sealing would be achieved with model parameters appropriate for a low-permeability quartzite. However, we are unable to reproduce flow rates measured during experiments on granites, where sealing was incomplete. Furthermore, our results indicate that silica concentrations of the outlet fluid approach quartz saturation as the sample sealed; the measured concentrations did not change substantially and remained supersaturated through the length of the experiments. Effects of reactions with feldspar and mica are probably important. Because only small amounts of fluid were collected, aluminum concentrations could not be measured. Without this information and more complete kinetic data, the behavior of these minerals cannot be quantitatively examined. Order-of-magnitude calculations suggest that feldspar dissolution alone can account for observed silica concentrations and measured differences between the 250° and 300°C experiments, assuming that porosity reductions are governed entirely by the formation of clays--that is, no silica precipitates. In addition, at least three important parameters--dispersivity, flow porosity and mineral surface area--are either never or rarely measured. Further theoretical studies will require measurements of these properties.

REFERENCES.

Bird, R.B., W.E. Stewart and E.N. Lightfoot, 1960, Transport Phenomenon, John Wiley, New York, 780 p.

Facca, G., and F. Tonani, 1967, "The self-sealing geothermal field," Bull. Volcanology, 30, 271-273.

Fournier, R.O., and R.W. Potter, 1982, "An equation correlating the solubility of quartz in water from 25° to 900°C at pressures up to 10,000 bars," Geochim. Cosmochim. Acta, 46, 1969-1973.

Keenan, J.H., F. Keyes, P. Hill and J. Moore, 1978, Steam Tables, John Wiley, New York, 156 p.

Li, T. M. C., 1980, Axisymmetric Numerical Simulation of Hydrothermal Systems Including Changes in Porosity and Permeability due to the Quartz-Water Reaction, Ph.D. thesis, Penn. State Univ., 240 p.

Lichtner, P.C., H.C. Helgeson and K. Pruess, 1983, "Numerical modeling of fluid flow with simultaneous chemical reaction in hydrothermal systems," Geol. Soc. Am. Abstr.with Prog., 15, p. 627.

Lockner, D., D. Bartz and J. Byerlee, 1978, "Change in permeability during flow of water through granite subjected to a temperature gradient," Proc. Fourth Stanford Geothermal Workshop.

Moore, D.E., C.A. Morrow and J.D. Byerlee, 1981, "SiO_2 precipitation accompanying fluid flow through granite held in a temperature gradient," Proc. Seventh Stanford Geothermal Workshop.

_____, 1983, "Chemical reactions accompanying fluid flow through granite held in a temperature gradient," Geochim. Cosmochim. Acta, 47, 445-453.

Morrow, C.A., D. Lockner, D. Moore and J. Byerlee, 1981, "Permeability of granite in a temperature gradient," J. Geophys. Res., 86, 3002-3008.

Nguyen, V.V., W.G. Gray, G.F. Pinder, J.F. Botha and D.A. Crerar, 1982, "A theoretical investigation on the transport of chemicals in reactive porous media," Water Resources Res., 18, 1149-1156

Rimstidt, J.D., and H.L. Barnes, 1980, "The kinetics of silica-water reactions," Geochim. Cosmochim. Acta, 44, 1683-1699.

Rubin, Jacob, 1983, "Transport of reacting solutes in porous media: relation between mathematical nature of problem formulation and chemical nature of reactions," Water Resources Res., 19, 1231-1252

Summers, R., K. Winkler and J. Byerlee, 1978, "Permeability changes during the flow of water through Westerly granite at temperatures of 100°-400°C," J. Geophys. Res, 83, 339-344.

Touloukian, Y.S., W.R. Judd and R.F. Roy, 1981, Physical Properties of Rocks and Minerals, McGraw-Hill, New York, 548 p.

Turcotte, D.L., and G. Schubert, 1982, Geodynamics, John Wiley, New York, 450 p.

Watson, J.T.R., R.S. Basu and J.V. Sengers, 1980, "An Improved equation for the viscosity of water and steam," in Water and Steam: Their Properties and Current Industrial Applications, J. Straub and K. Scheffler, eds., Pergamon Press, New York, p. 336-343.